High speed, wide velocity dynamic range Doppler optical coherence tomography (Part II): Imaging *in vivo* cardiac dynamics of *Xenopus laevis*

Victor X.D. Yang[1], Maggie L. Gordon[1], Emily Seng-Yue[3], Stewart Lo[3], Bing Qi[3], Julius Pekar[3], Alvin Mok[3], Brian C. Wilson[1,3,4] and I. Alex Vitkin[1,2,3]

Depts. of [1]Medical Biophysics and [2]Radiation Oncology, University of Toronto, Toronto, ON M5G 2M9, Canada
[3]Ontario Cancer Institute/University Health Network, Toronto, ON M5G 2M9, Canada
[4]Biophotonics Facility, Photonics Research Ontario, Toronto, ON M5G 2M9,Canada
yangx@uhnres.utoronto.ca

Abstract: We previously reported a Doppler optical coherence tomography (DOCT) system design [1] for high-speed imaging with wide velocity dynamic range (up to 28.5 dB when acquiring 8 frames per second), operating at 1.3 μm with a coherence length of 13.5 μm. Using a developmental biology model (*Xenopus laevis*), here we test the DOCT system's ability to image cardiac dynamics in an embryo *in vivo*, with a simple hand-held scanner at 4 ~ 16 frames per second. In particular, we show that high fidelity DOCT movies can be obtained by increasing the reference arm scanning rate (~8 kHz). Utilizing a combination of four display modes (B-mode, color-Doppler, velocity variance, and Doppler spectrum), we show that DOCT can detect changes in velocity distribution during heart cycles, measure the velocity gradient in the embryo, and distinguish blood flow Doppler signal from heart wall motions.

OCIS codes: (110.4500) Optical Coherence Tomography; (170.3880) Medical and biological imaging; (170.1650) Coherence imaging; (100.6950) Tomographic image processing

References

1. V. X. Yang, M. L. Gordon, B. Qi, J. Pekar, S. Lo, E. Seng-Yue, A. Mok, B. C. Wilson, and I. A. Vitkin, "High speed, wide velocity dynamic range Doppler optical coherence tomography (Part I): System design, signal processing, and performance," Opt. Express **11,** 794-809 (2003), http://www.opticsexpress.org/abstract.cfm?URI=OPEX-11-7-794.
2. D.Huang, E.A.Swanson, C.P.Lin, J.S.Schuman,W.G.Stinson, W.Chang, M.R.Hee, T.Flotte, K. Gregory, C.A.Puliafito, and J.G.Fujimoto, "Optical coherence tomography," Science **254**, 1178-81 (1991).
3. S. A. Boppart, G. J. Tearney, B. E. Bouma, J. F. Southern, M. E. Brenzinski, and J. G. Fujimoto, "Noninvasive assessment of the developing Xenopus cardiovascular system using optical coherence tomography," Proc. Natl. Acad. Sci. **94**, 4256-61 (1997).
4. S. Yazdanfar, M.D. Kulkarni, and J.A. Izatt, "High resolution imaging of *in vivo* cardiac dynamics using color Doppler optical coherence tomography," Opt. Express **1**, 424-31 (1997), http://www.opticsexpress.org/abstract.cfm?URI=OPEX-1-13-424.
5. G.J. Tearney, B.E. Bouma, and J.G. Fujimoto, "High-speed phase- and group-delay scanning with a grating-based phase control delay line," Opt. Lett. **22(23)**, 1811-3 (1997).
6. A.M. Rollins, M.D. Kulkarni, S. Yazdanfar, R. Ung-arunyawee, and J.A. Izatt, "*In vivo* video rate optical coherence tomography," Opt. Express **3,** 220-29 (1998), http://www.opticsexpress.org/abstract.cfm?URI=OPEX-3-6-219.
7. V.Westphal, S.Yazdanfar, A.M.Rollins, and J.A.Izatt, "Real-time, high velocity-resolution color Doppler optical coherence tomography", Opt. Lett. **27(1)**, 34-6 (2002).
8. V.X.D.Yang, M.L.Gordon, A.Mok, Y.Zhao, Z.Chen, R.S.C.Cobbold, B.C.Wilson, and I.A.Vitkin, "Improved phase-resolved optical Doppler tomography using the Kasai velocity estimator and histogram segmentation," Opt. Comm. **208**, 209-214 (2002).
9. G. J. Tearney, M. E. Brezinski, B. E. Bouma, S. A. Boppart, C. Pitris, J. F. Southern, and J. G. Fujimoto, "In vivo endoscopic optical biopsy with optical coherence tomography," Science **276**, 2037-9 (1997).
10. P. D. Nieuwkoop, and J. Faber, *Normal Table of Xenopus laevis (Daudin)*, Garland, New York (1994).
11. J.A.Jensen, *Estimation of blood velocities using ultrasound* (Cambridge, 1996).

#2520 - $15.00 US Received May 29, 2003; Revised June 30, 2003

12. S. J. Kolker, U. Tajchman, and D. L. Weeks, "Confocal imaging of early heart development in *Xenopus laevis*," Develop. Biol. **218**, 64-73 (2000).

1. Introduction

Optical coherence tomography (OCT) [2] has been used to study the embryo (tadpole) of *Xenopus laevis* (the South African clawed frog), in particular its cardiovascular system [3]. Under *in vitro* conditions, fine microstructural details such as the trabeculae carneae of the heart wall were visualized in the developing *Xenopus* heart, displaying 2-dimentional reflectance images (analogous to B-mode ultrasound) at ~ 12 μm axial resolution. *In vivo* imaging of the embryo heart at up to 4 frames per second (fps) showed the dynamics of the cardiac cycle to a limited extent, but the temporal resolution was not adequate to fully ascertain the heart motion. When operating in optical cardiogram mode (displaying 1-dimentional reflectance as a function of time, analogous to M-mode ultrasound), higher temporal resolution enabled measurement of dynamic cardiac parameters such as the ejection time, but only with information collected along a single axial scan line. In addition to structural information, blood flow in the embryo heart can be quantified by extending OCT with Doppler flow measurement techniques [4]. Velocity resolution of ~ 500 μm/s had been achieved under *in vivo* conditions when imaging the *Xenopus* embryonic heart; however, the slow reference arm scanning rate of the early Doppler OCT systems prevented acquisition of color-Doppler movies at real-time frame rates. Nonetheless, using a post-processing technique, blood flow in the heart was visualized at ~ 5 fps, demonstrating the feasibility of color-Doppler OCT imaging of cardiac dynamics. With the development of rapid scanning optical delay (RSOD) [5], video rate structural OCT imaging has been applied to *Xenopus* embryos, at frame rates up to 32 fps with 250 × 125 pixels [6]. Consequently, RSOD equipped Doppler OCT demonstrated real-time (8 fps) imaging of the *Xenopus* embryo heart, with a velocity resolution (expressed in minimum resolvable Doppler shift frequency) of 300 Hz, equivalent to 0.4 mm/s blood flow at 70° Doppler angle [7]. Due to the ease of handling, *Xenopus laevis* has become a benchmark specimen for demonstrating OCT system performance under *in vivo* conditions [6,7].

Previously, we reported a Doppler optical coherence tomography (DOCT) system design [1] for high-speed imaging (up to 32 frames per second), operating at 1.3 μm with a coherence length of 13.5 μm in air using an 8 kHz RSOD. We also used velocity histogram segmentation to reduce motion artefacts, commonly encountered in Doppler OCT imaging [8]. While maintaining the minimum resolvable Doppler shift frequency of ~ 300 Hz when imaging at 8 fps, the maximum detectable Doppler shift has been increased to ± 4 kHz (equivalent to bi-directional flow of ± 4 mm/s at 60° Doppler angle) without aliasing effects. This improvement in the velocity dynamic range (~ 28.5 dB) can result in enhanced ability for imaging blood flow dynamics. Hence, in this paper, we use the *Xenopus laevis* model to demonstrate the wide velocity dynamic range DOCT system's performance in imaging dynamic blood flow.

2. Material and methods

2.1 DOCT system

A detailed description of the DOCT system is given in the preceding companion paper [1]. Briefly, a broadband light source (JDS, Ottawa ON, Canada) with a polarized output power of 5 mW at a center wavelength λ_0 = 1.3 μm and bandwidth of $\Delta\lambda$ = 63 nm is used. An optical circulator (O-Net, Boston, MA) is used to increase the signal-to-noise ratio (SNR). The system uses a Michelson interferometer configuration with a RSOD operating at 8 kHz in the reference arm, and a hand-held scanner in the sample arm. As shown in Fig. 1, the hand-held scanner consists a fiber probe tip at the end of a SMA-28 fiber, attached to a rotor disk. The disk has been machined with inertia matching to a galvanometer (Cambridge Technology,

#2520 - $15.00 US Received May 29, 2003; Revised June 30, 2003

Cambridge, MA), providing stable scanning at frequencies up to 250 Hz. Within the fiber probe, an angel polished (8°) gradient index (GRIN) lens is bonded to the polished end of the fiber with optical adhesive. The focal spot diameter is ~ 25 μm, with a depth of focus ~ 1.2 mm. For better mechanical strength, a steel sheath (outer diameter ~ 1.1 mm, inner ~ 1.0 mm) encloses the lens-fiber assembly and allows attachment to the rotor disk.

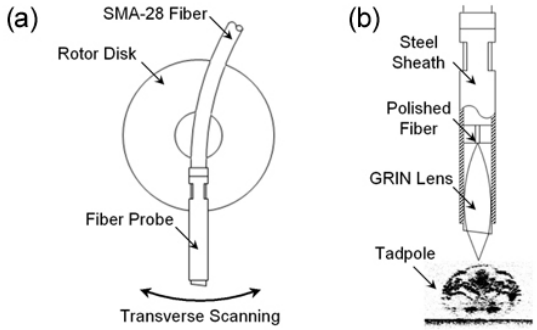

Fig. 1. (a) Schematics of the hand-held probe, incorporating a fiber probe at the end of a SMA-28 fiber, and a rotor disk connected to a galvanometer scanner. (b) Details of the fiber probe. An angle-polished GRIN lens with ~ 1 mm working distance is bonded to the polished fiber end using optical cement. The entire assemble is housed in a steel sheath of 1.1 mm outer diameter.

This hand-held scanner design is smaller and simpler than those used previously in tadpole imaging [7], with less optical surfaces in the beam path, which should reduce the internal back reflectance of the sample arm. The fiber probe tip resembles the endoscopic OCT probe design of Tearney *et al* [9], without using a prism to deflect the beam. One disadvantage of this simplified design is the angular distortion; however, the transverse scanning range for the application of tadpole imaging can be kept to less than 3 mm, making the distortion unnoticeable. When using a saw-tooth pattern, transverse scans can be acquired at frequencies beyond 50 Hz. If repeatable imaging at a particular location is required, this scanner can also be mounted on the optical table.

As previously described [1], the detected OCT signal is demodulated into in-phase (I) and quadrature (Q) components. The structural or B-mode image pixel intensity is calculated by:

$$\left\langle S^2 \right\rangle = \frac{1}{MN}\sum_{m=1}^{M}\sum_{n=1}^{N}\left[I_{m,n}^2 + Q_{m,n}^2\right] \tag{1}$$

, where M and N denote the number of pixels to average in the axial and transverse directions, respectively. The color-Doppler mode displays the mean Doppler shift frequency induced by moving reflectors, as the following,

$$f_D = \frac{f_a}{2\pi}\arctan\left\{\frac{\frac{1}{M(N-1)}\sum_{m=1}^{M}\sum_{n=1}^{N-1}\left(I_{m,n+1}Q_{m,n} - Q_{m,n+1}I_{m,n}\right)}{\frac{1}{M(N-1)}\sum_{m=1}^{M}\sum_{n=1}^{N-1}\left(Q_{m,n+1}Q_{m,n} + I_{m,n+1}I_{m,n}\right)}\right\} = \frac{f_a}{2\pi}\arctan\left\{\frac{\langle Y\rangle}{\langle X\rangle}\right\}, \tag{2}$$

where f_a = 8 kHz is the RSOD scanning frequency. Finally, the normalized velocity variance can be calculated as:

#2520 - $15.00 US
Received May 29, 2003; Revised June 30, 2003

$$\frac{\sigma_v^2}{f_a^2} = \left(1 - \frac{\sqrt{\langle X \rangle^2 + \langle Y \rangle^2}}{\langle S^2 \rangle} \right), \tag{3}$$

which can be used to distinguish turbulent flow (high variance) from block tissue motion (low variance). The blood-flow induced Doppler shift frequency can also be presented in audio format. By calculating the Doppler frequency spectrum from the *I* and *Q* signals [1] and inverse Fourier transforming the spectrum, stereo audio output is obtained to represent forward and reverse blood flow.

2.2 Xenopus laevis model

Stage 45~47 [10] *Xenopus* tadpoles were anesthetized in ~ 0.01% Tricaine until they no longer responded to touch or vibrations. The tadpole was transferred into a petri dish, submerged in shallow water with the ventral side up for DOCT imaging. The petri dish was placed on a x-y-z translation stage, allowed easy positioning of the tadpole. For better *en face* visualization and understanding of the *Xenopus* anatomy, *in vivo* autofluorescence laser scanning confocal microscopy was performed using a Zeiss microscope (Axiovert 100 – LSM 510, Carl Zeiss Canada) with 351 nm excitation light and a 385 nm long pass filter.

3. Results and discussion

An example set of confocal images is shown in Fig. 2, illustrating the detailed anatomy of the *Xenopus* tadpole at stage 47 and the relative locations of DOCT imaging.

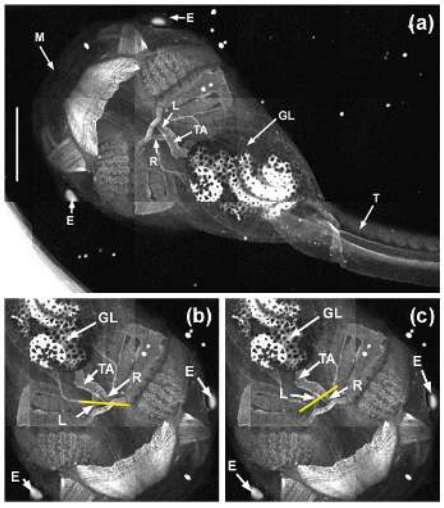

Fig. 2. (a) UV excited autofluorescence confocal micrograph of stage 47 *Xenopus* tadpole, showing the ventral (chest) side anatomy including mouth (M), eyes (E), tail (T), and gut loop (GL). Embryonic heart structures such as truncus arteriosis (TA), and the left and right aortic branches (L and R) are also visible. Scale bar = 2 mm. (b) Location (marked by yellow line) for cross-sectional DOCT imaging, shown in Fig. 3. (c) Location (yellow line) for cross-sectional DOCT imaging, shown in Fig. 5.

Due to the rapid contraction of the heart, blood flow in the left and right aortic branches (L and R) is pulsatile and brief, which represents a perfect target to test the DOCT system's performance. As shown in Fig. 2(b) and Fig. 3, the imaging plane was aligned to intersect the L at approximately normal, and tangentially cut across R. This view allowed cross-sectional visualization of the blood flow in L, as well as determination of the Doppler angle ($\alpha \approx 63°$) in R for absolute flow velocity calculation. During systole (contraction), the peak Doppler shift frequency in R was ~ 1 kHz, with the velocity gradient visible, as shown in the video

#2520 - $15.00 US Received May 29, 2003; Revised June 30, 2003

(Fig. 3). This gradient confirmed that the Doppler shift was aliased slightly over one cycle, reaching ~ 9 kHz. Hence, the peak flow velocity can be quantified as

$$\langle v \rangle = \frac{\lambda_0 f_D}{2 n_t \cos(\alpha)} \approx 9 \text{ mm/s}, \tag{4}$$

where the tissue index of refraction n_t is the assumed to be 1.4.

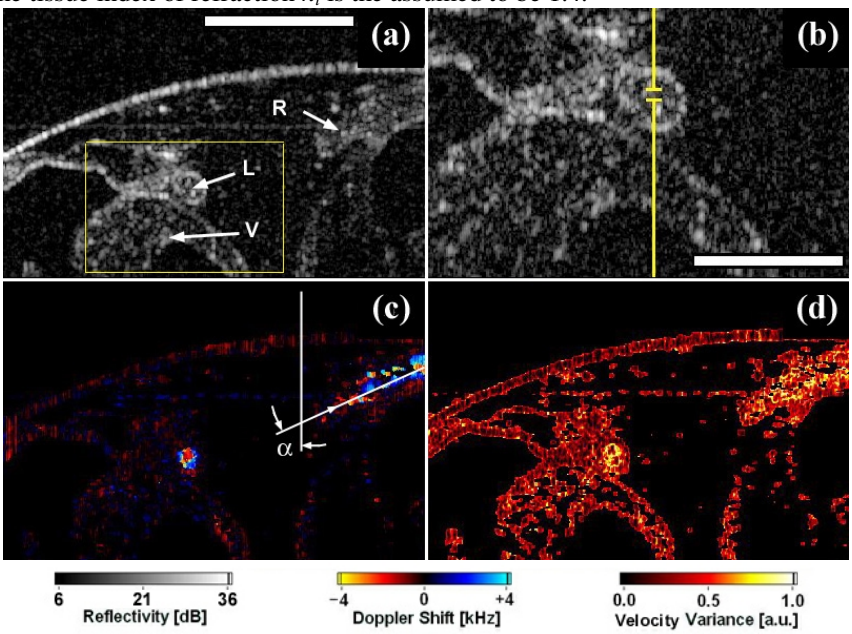

Fig. 3. DOCT video [480 kB with audio] of a stage 47 *Xenopus* tadpole, imaging the left and right aortic branches (L and R), acquired at 8 fps. (a) Structural (B-mode) video of the aortic branches cross-section. Notice a smaller vessel (V) in the video. Bar = 500 µm. (b) 2× zoom of the yellow rectangular region in (a), showing the micro-structure of L. The break in the yellow line indicates the location from which Doppler spectrum information is collected and encoded into audio format (see Fig. 4), demonstrating the velocity distribution within L. Bar = 250 µm. (c) Color-Doppler video, showing the corresponding velocity map in the cross-section. Notice the low noise background, and the pulsatile blood flow in L and R. The Doppler angle (α) is estimated to be ~ 63° for R. The small blood vessel (V) is much better visualized in the color-Doppler mode, allowing estimation of its diameter to be less than 70 µm. Systole occurs during the 4th and 5th frames, where the velocity gradients in R are visible, and the peak Doppler shift is ~ 9 kHz considering aliasing effects. (d) Velocity variance video, showing the increased variance of the blood flow within L and R. Each individual image was recorded at 450 × 508 pixels, and re-sampled into 256 x 160 pixels for video compression. The faint horizontal line in (a), (c), and (d) was an artefact probably due to multiple-reflection.

The audio signal accompanying the video in Fig. 3 was calculated from a separate recording, immediately after the video acquisition, when the transverse scanning was paused at the position marked by the yellow vertical line intersecting L in Fig. 3(b). The *I* and *Q* signals collected at the center of L were used to compute the Doppler spectrum (Fig. 4), and then inverse Fourier transformed to obtain the stereo audio. Due to the large signal dynamic range, the Doppler spectrum is displayed as the logarithmic of the spectral intensity. As shown in Fig. 4, the onset of systole was rapid (< 50 ms), with a broad range of velocity components, although the heart rate was only about 0.6 beat per second. The peak velocity component caused aliasing, resulting in Doppler shift frequencies beyond 8 kHz, which was consistent with the color-Doppler video. The temporal extent of the systole event was less than 200 ms full width half max, suggesting that a frame rate of at least 5 Hz is required to visualize the event.

#2520 - $15.00 US
Received May 29, 2003; Revised June 30, 2003

In clinical ultrasound systems, images similar to Fig. 3 and 4 can be acquired simultaneously using multi-element transducers. With a single element transducer, it is possible to obtain simultaneous results with a reduction in either the color-Doppler frame rate or the spectral resolution in the Doppler spectra [11]. At the present time, we chose to pause the transverse scanning and obtain the Doppler spectra with high fidelity at 8 kHz sampling rate (equivalent to the axial scan frequency). In the future a multi-element DOCT system may overcome this limitation.

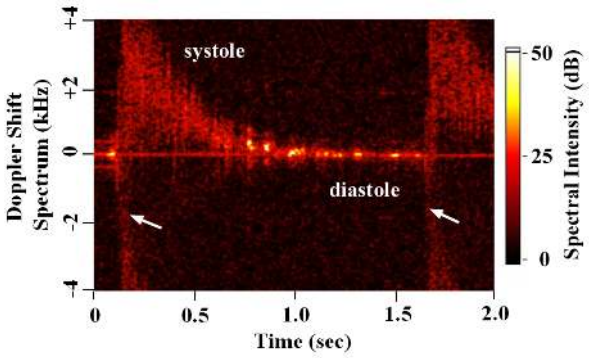

Fig. 4. Doppler spectral display of the DOCT system. The full Doppler spectrum represents the velocity distribution of the blood flowing within the analysis window, which is the gap in the yellow line shown in Fig. 3(b). Notice the rapid onset of systole and the aliasing caused by the peak velocity (arrows), as well as the relatively longer time for diastole (heart relaxation).

As demonstrated previously using flow phantoms [1], increasing DOCT frame rate degrades the accuracy of velocity estimation, accompanied by increased noise in the images. Fig. 5 shows a series of DOCT videos, acquired at different frame rates, with the imaging plane indicated as in Fig. 2(c). It is evident that thin structure such as the pericardium (P) becomes harder to identify as the frame rate increases. Figs. 5(a), (b) and (c) are composite videos with the color-Doppler image overlaid on the B-mode image. The overlay operation performed by post-processing, due to a more complex motion segmentation algorithm employed here. In addition to the structural intensity and velocity thresholds used previously [4,7], a 7×7 median filter was applied spatially to reject velocity noise. The main advantage of this technique is that it allows better visualization of motion arising from weakly backscattering targets such as red blood cells, by using reduced intensity and velocity thresholds. The disadvantage is the higher computational complexity, which can be addressed in the future by hardware digital signal processing.

#2520 - $15.00 US Received May 29, 2003; Revised June 30, 2003

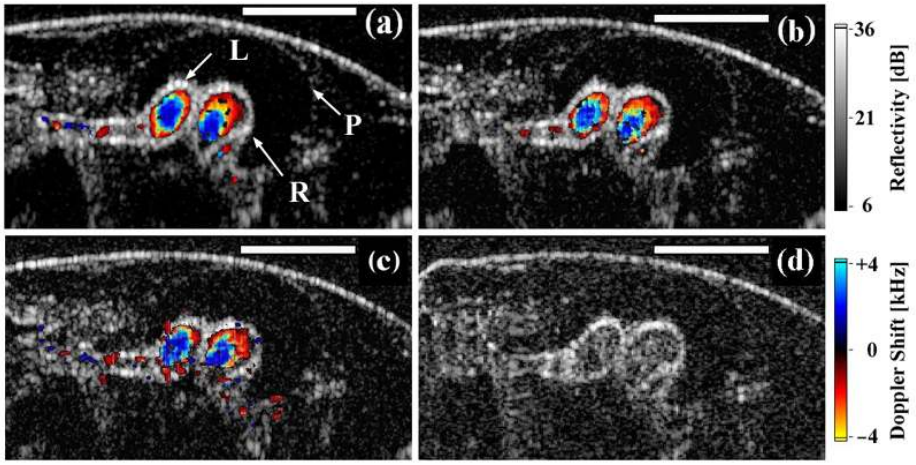

Fig.5. High-speed videos acquired at different frame rates: (a) 4 fps [213 kB], (b) 8 fps [231 kB], (c) 16 fps [473 kB], and (d) 32 fps [1.5 MB]. Videos (a)-(c) were acquired at 450 × 508 pixels, and (d) was acquired at 225 × 508 pixels, before re-sampling for compression. Scale bar = 500 μm. Notice the reduction in SNR as frame rate increases. P: pericardium. L and R: left and right aortic branches. No Doppler processing was performed in (d) due to excessive noise.

At lower frame rates (4 ~ 8 fps), the velocity gradient within the left and right aortic branches can be clearly visualized, with little motion artefacts in the surrounding tissue. At 16 fps, considerably more noise in both the structural image and velocity estimation can be seen. However, it is still possible to visualize the velocity gradient in the blood flow. At 32 fps, no velocity estimation was attempted due to excessive noise and only the structural image is shown in Fig. 5(d). The movement of red blood cells through the aortic branches can still be visualized as the rapidly changing speckle patterns of the blood flow, which are different from that in the surrounding tissue.

The high-speed B-mode video can also be used to ascertain the dynamic sequence of events during the cardiac cycle, which can be challenging in the small *Xenopus*. It is difficult to identify the different components of the heart since they are in complex motion, including simultaneous contraction, displacement, and recoil.[1] Fig. 6 shows the atria, ventricle, and truncus arteriosis of a stage 46 *Xenopus* heart, with the ventral side facing up.

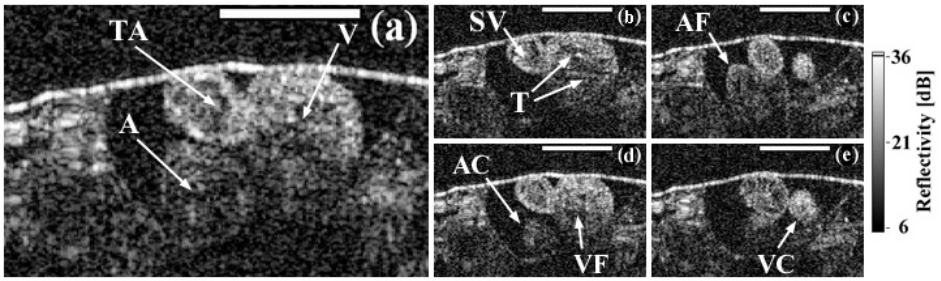

Fig.6. (a) Real-time (32 fps) B-mode OCT video [914 kB] of the *Xenopus* heart, showing the ventricle (V), atria (A), and the truncus arteriosis (TA). (b) Same video played back at 10 fps [246 kB], allowing better visualization of the motion dynamics, as well as the spiral valve (SV) in TA and the trabeculae carneae (T) network in the ventricle. Static frames in (c)-(e) illustrate different phases of the heart cycle, showing the sequence of atria filling in (c), atria contraction

[1] Previous *ex vivo* confocal microscopy studies of *Xenopus* using fluorescent antibodies [12] have shown that the truncus arteriosis is the most ventral component, and the atria are the most dorsal components. However, such information is insufficient for *in vivo* identification since it is uncertain whether the *Xenopus* heart retains its anatomical orientation after cardiac arrest. This problem can be abrogated with high-speed B-mode imaging at 32 fps.

#2520 - $15.00 US Received May 29, 2003; Revised June 30, 2003

(AC) and ventricle filling in (d), and ventricle contraction (VC) which pumps blood through the truncus arteriosis in (e). Acquired at 225 × 508 pixels before re-sampling for video compression. Scale bar = 500 μm.

By visualizing the filling and contraction sequence, one can confirm that the most ventral component in Fig. 6 is indeed the truncus arteriosis, which links the ventricle to the aortic branches. This is consistent with the fluorescence confocal microscopy. It is interesting that micro-structures such as the spiral valve in the truncus arteriosis and trabeculae carneae network in the ventricle can also be visualized under dynamic imaging, with their anatomical positions consistent with those found in *ex vivo* studies [12].

The blood flow through the spiral valve can be better seen in color-Doppler and velocity variance modes, which are illustrated by the video in Fig. 7. When the ventricle contracts, blood is forced through the truncus arteriosis by extending its wall and flowing around the spiral valve, which remains open for approximately 250 ms. The blood flow through the valve is probably turbulent, as suggested by the color-Doppler images in Fig. 7(b). Distinct from the turbulent blood flow, cardiac muscle motion can also be seen in the color-Doppler images, with a relatively homogeneous pattern. This is confirmed by the velocity variance image in Fig. 7(c), showing high variance in the blood flow and low variance in the muscle walls. Thinner (~ 60 μm) walls of the truncus arteriosis can also be visualized in the zoomed images of Figs. 7(d) and (e).

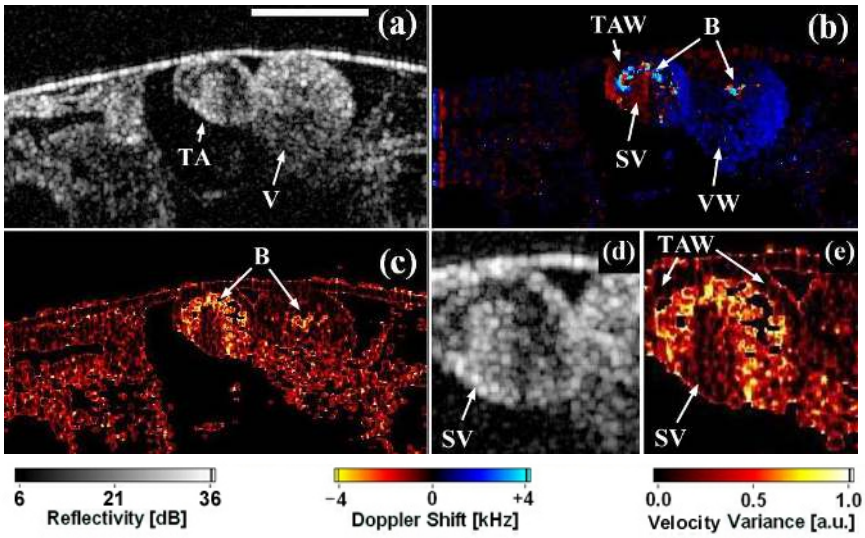

Fig.7. DOCT video of the stage 46 *Xenopus* tadpole heart, acquired at 8 fps [305 kB]. (a) Structural video showing the ventricle (V) and truncus arteriosis (TA). The atria are also visible in the video (not shown in this static frame). Scale bar = 500 μm. (b) Color-Doppler video showing the blood flow (B) within the ventricle and the truncus arteriosis. Notice the homogeneous distribution of Doppler shift in the ventricle wall (VW) and the truncus arteriosis wall (TAW). The partial division at the center of truncus arteriosis is probably the spiral valve (SA), also showing homogeneous Doppler shift distribution, distinct from the blood flow. A small blood vessel can also be seen in the video (not shown in this static frame). (c) Velocity variance video showing the blood flow (B). The blood flow, spiral valve, and the truncus arteriosis wall are better visualized in the 2 × zoom videos, shown in structural mode (d), and velocity variance mode (e). Acquired at 450 × 508 pixels per frame before re-sampling for video compression.

The high SNR in these images and videos is the result of specialized hardware and software signal processing, described in detail previously [1]. The high reference scanning frequency (8 kHz) is critical for increasing the velocity dynamic range for clear visualization

#2520 - $15.00 US Received May 29, 2003; Revised June 30, 2003

of the velocity gradients. The high scanning frequency is also required for high speed imaging (up to 32 fps) with adequate number of transverse lines per frame. In addition, the velocity sensitivity is maintained at high frame rates by increasing the number of lines averaged. Hence, it is clear that high reference scanning frequency is essential for good quality DOCT imaging.

The velocity noise at high frame rates (16 ~ 32 fps) is problematic, but we believe this is largely due to speckle modulation caused by the rapid transverse scanning. A number of strategies are available to resolve this issue. One is to use a larger diameter focal spot in the sample arm, with a trade-off in reduced spatial resolution. Another is to reduce the transverse scanning speed, with a trade-off in field of view. We are currently constructing a multi-channel DOCT probe, which reduces the transverse scanning speed proportional to the number of channels, while maintaining the imaging field of view, operating at high frame rates.

Detection of the velocity gradient, as shown by the colored-rings in Fig. 5, is important for several reasons. Besides allowing distinction between lamina and turbulent flows, reliably resolved velocity gradient can be used to calculate the shear rate in blood vessels. In addition, phase unwrapping techniques can be used with confidence to extrapolate the true Doppler shift from aliased values, when the velocity gradient is visible. This can be used to extend the velocity detection range.

In clinical ultrasound, a longer pulse train is used for Doppler imaging since it provides better velocity estimation, while a shorter pulse train is used for high spatial resolution B-mode imaging. A similar argument can be made in DOCT that probably B-mode and Doppler imaging should be performed with different coherence lengths light sources. We are exploring the possibility of a hybrid DOCT system, using a femto-second light source for ultrahigh resolution B-mode imaging and a super luminescent diode source for the Doppler modes. The resultant system will have the advantage of concurrent high spatial and velocity resolutions, in addition to the ability of independent scanning patterns for the B-mode and Doppler modes.

4. Conclusions

In conclusion, we have demonstrated a DOCT system capable of imaging the cardiac dynamics of *Xenopus laevis* with high frame rate and wide velocity dynamic range. High fidelity color-Doppler imaging of the *Xenopus* heart has shown that DOCT can quantitatively measure blood flow speed as high as 9 mm/s, with velocity noise as low as 300 Hz (~ 150 μm/s), while visualizing the dynamic cardiac events at 8 frames per second. Velocity gradients in the blood flow can be clearly imaged at high speed up to 16 frames per second. The full velocity distribution in the blood flow, at different phases of the cardiac cycle, can be measured in the Doppler spectrum mode and presented in stereo audio. Using this DOCT system, we demonstrated identification of the anatomical components of the *Xenopus* heart during complex cardiac motion, while distinguishing pulsatile blood flow from heart wall movements.

Acknowledgement

The authors would like to thank Dr. Winklbauer and his staff in the Department of Zoology, University of Toronto for providing the specimens and advice on experimental protocols. We are grateful to N. Munce for his assistance with the confocal microscopy. This work was supported by the Natural Science and Engineering Research Council of Canada, the Canadian Institutes for Health Research, the Canadian Cancer Society through a grant from National Cancer Institute of Canada, the Canadian Foundation for Innovation, Photonics Research Ontario, and a donation from the Gordon Lang Foundation.